Available online at www.sciencedirect.com
ScienceDirect
Applied Catalysis B: Environmental 76 (2007) 82–91
APPLIED CATALYSIS B: ENVIRONMENTAL
www.elsevier.com/locate/apcatb

# Nanocrystalline anatase $TiO_2$ photocatalysts prepared *via* a facile low temperature nonhydrolytic sol–gel reaction of $TiCl_4$ and benzyl alcohol

Jian Zhu [a], Jun Yang [a], Zhen-Fen Bian [b], Jie Ren [b], Yong-Mei Liu [a], Yong Cao [a,*], He-Xing Li [b], He-Yong He [a], Kang-Nian Fan [a,*]

[a] *Department of Chemistry and Shanghai Key Laboratory of Molecular Catalysis and Innovative Materials, Fudan University, Shanghai 200433, PR China*
[b] *Department of Chemistry, Shanghai Normal University, Shanghai 200234, PR China*

Received 17 January 2006; received in revised form 9 May 2007; accepted 12 May 2007
Available online 17 May 2007

**Abstract**

Nanocrystalline anatase $TiO_2$ photocatalysts prepared by a facile nonhydrolytic sol–gel (NSG) reaction of $TiCl_4$ and benzyl alcohol at low temperature, followed by subsequent calcination at elevated temperatures were investigated in relation to their performance in the photocatalytic degradation of phenol. A variety of techniques including $N_2$ adsorption, X-ray powder diffraction (XRD), diffuse reflectance FTIR spectroscopy (DRIFTS), thermogravimetric measurements (TG/DTA), transmission electron micrographs (TEM), and X-ray photoelectron spectroscopy (XPS) were employed to characterize the resulting materials. It is shown that the fresh nanocrystalline $TiO_2$ sample obtained by the low temperature NSG process exhibits considerable activity comparable to that of commercial photocatalyst Degussa P-25, although evidence shows it to be surface-capped with appreciable amount of organic moieties. Moreover, it is demonstrated that the catalytic efficiency of the as-prepared nanocrystalline $TiO_2$ sample can be further markedly enhanced by subsequent thermal treatment at elevated temperatures ranging from 300 to 600 °C. Both the calcination temperature and calcination time appear to be crucial factors in influencing a number of critical properties of the calcined $TiO_2$ samples such as the surface area, particle size, crystallinity, amount of surface hydroxyl groups, as well as carbonaceous residues. The $TiO_2$ photocatalyst obtained by calcination at 400 °C for 3 h exhibits the highest activity toward photocatalytic degradation of phenol.


*Keywords:* Photocatalytic; $TiO_2$; Nonhydrolytic; Sol–gel; $TiCl_4$; Benzyl alcohol

## 1. Introduction

Currently, titanium dioxide has been one of the most studied semiconductors for photocatalytic reactions due to its low cost, ease of handling, and high resistance to photoinduced decomposition [1–6]. An important aspect in the preparation of $TiO_2$ photocatalysts for environmental applications is the development of nanostructured $TiO_2$ powders with a number of favorable properties such as small particle size, high surface area, controlled porosity, and tailor-designed pore size distribution [2–4]. In particular, a number of recent literatures have focused on the preparation of mesoporous $TiO_2$ materials with high surface area and tailored framework structure using surfactant template [5,6]. Owing to their high surface-to-volume ratio and offering more easily accessible surface active sites, a further enhancement in the catalytic activity and process efficiency is expected [7].

In view of the synthetic methods developed for the preparation of nanostructured $TiO_2$, a wide variety of approaches including flame synthesis, ultrasonic irradiation, chemical vapor deposition, as well as sol–gel reactions have been reported [8–11]. Among them, sol–gel processes based on the hydrolysis and polycondensation of various titanium molecular precursors in aqueous solutions or an organic solvent have been shown to be especially versatile synthesis procedures [11–13]. The sol–gel processing can allow the formation of nanostructured materials with controlled porosity and shape (coatings, fibers, powders, monoliths) [12,14–16]. As a result, the design and fabrication of $TiO_2$-based photocatalysts by sol–gel processing has attracted increasing interest in recent years [17,18]. However, in most

* Corresponding authors. Tel.: +86 21 65643774/65643792-5; fax: +86 21 65642978.
*E-mail address:* yongcao@fudan.edu.cn (Y. Cao).

0926-3373/$ – see front matter © 2007 Elsevier B.V. All rights reserved.
doi:10.1016/j.apcatb.2007.05.017

cases, the sol–gel derived precipitates at low temperatures are amorphous in nature, which generally do not possess photocatalytic activity, and ultrasonic irradiation. Thereby, subsequent hydrothermal processing, or calcination is necessary to induce crystallization [19–22].

On the other hand, it is also well documented that the performance of a $TiO_2$ photocatalyst is strongly dependent on a number of other structural factors such as crystal phase as well as the degree of crystallinity of the $TiO_2$ particles [23]. In this respect, it is beneficial to develop new improved methods that can allow the direct synthesis of crystalline $TiO_2$ nanostructures at ambient or low temperatures since further heating at high temperatures often leads to undesirable rapid increase of the particle size accompanied by significant loss of surface area and porosity. One distinctly attractive advantage associated with such processes is the energy saving in the preparation steps. Additionally, such procedures could also allow for a wider selection of support materials such as cotton, wood or plastic, where a low temperature treatment is favored for preparing $TiO_2$-immobilized samples [24].

During the last decades, several nonhydrolytic sol–gel (NSG) methods involving the reaction of titanium chloride ($TiCl_4$) with a variety of different oxygen donor molecules that can allow the direct formation of highly crystalline $TiO_2$ powders based on ''alkyl halide elimination'' at low temperatures have been developed [25,26]. By varying the nature of the oxygen donor (alcohol or ether), a variety of crystalline polymorphs of $TiO_2$ such as anatase and rutile nanoparticles have been successfully prepared by these methods [27]. Despite the excellent potentialities of nonhydrolytic routes for the preparation of highly crystalline titanium oxides, there have been very few studies on the photocatalytic performances of nanocrystalline $TiO_2$ derived from these routes. Very recently, Fox et al. demonstrated that nanoscaled $TiO_2$ powders with high photocatalytic oxidation activities could be prepared by a nonhydrolytic acylation/deacylation of titanium alkoxide precursors in supercritical carbon dioxide [28]. However, the supercritical/nonhydrolytic approach described by Fox et al. can only afford the generation of organic-capped amorphous $TiO_2$ powders at ambient temperatures. To obtain a crystalline sample possessing high photocatalytic activity, a further calcination of the as-obtained material at 500 °C for 5 h is still needed.

In the present study, we report that highly photoactive nanocrystalline anatase $TiO_2$ with tailored control of the surface nature and microstructural properties can be synthesized by a modified NSG method based on a low temperature solution-based reaction of titanium chloride ($TiCl_4$) and benzyl alcohol (Scheme 1). In particular, special attention has been paid to the effect of calcination on the surface and microstructural properties as well as the photoactivities of the thermally processed nanocrystalline $TiO_2$ materials derived by the NSG method. A comparison of the photocatalytic properties of the present nanocrystalline $TiO_2$ samples with that of commercial photocatalyst Degussa P-25 was also presented.

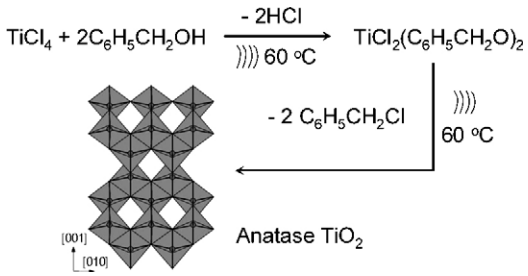


Scheme 1. Synthesis of nanocrystalline $TiO_2$ by low temperature nonhydrolytic alcoholysis/polycondensation of titanium chloride ($TiCl_4$) by benzyl alcohol.

## 2. Experimental

### 2.1. Sample preparation

The nanocrystalline $TiO_2$ catalysts reported in this study have been prepared by minor modification of a previously reported procedure developed by Niederberger et al. using the NSG reactions of benzyl alcohol and $TiCl_4$ at low temperatures [29]. In a typical preparation, 4 mL $TiCl_4$ (99.9%) was slowly dropped into 80 mL benzyl alcohol (99.8%, anhydrous) bathed at 0 °C under argon protection. After stirring for 30 min, the resulting translucent sol was aged at 60 °C under ultrasound irradiation (Brandson, 400 W/4 KHz). A white, thick suspension appeared within 8 h. The resulting white suspension was centrifuged followed by washing with acetone (2 mL × 50 mL) and THF (2 mL × 50 mL) for four times. After every washing step, the solvent was removed by centrifugation. The collected material was left to dry in air overnight and then ground into a fine white powder. Calcination of as-obtained samples was performed at elevated temperatures ranging from 300 to 800 °C for 1–12 h. The prepared samples were coded as NSG-*T*-*t* (see Table 1), where *T* and *t* refer to the calcination temperature and calcination time, respectively. A distinct difference of the present synthetic procedure from the conventional ''benzyl alcohol route'' proposed by Niederberger et al. [29] is the use of ultrasound irradiation during the ageing process to assist the low temperature alcoholysis/condensation reaction between benzyl alcohol and $TiCl_4$.

### 2.2. Sample characterization

The X-ray powder diffraction (XRD) of the samples was carried out on a Germany Bruker D8advance X-ray diffractometer using nickel filtered Cu Kα radiation with a scanning angle ($2\theta$) of 10–80°, and a voltage and current of 40 kV and 20 mA. The average size of anatase $TiO_2$ crystallites was estimated by means of the Scherrer equation from broadening of the (1 0 1) anatase reflection. Estimation of the content of anatase is based on: $X_A = 1/[1 + 1.265 I_R/I_A] \times 100\%$, where $I_A$ is the (1 0 1) peak intensity of anatase, $I_R$ is the (1 1 0) peak intensity of rutile, 1.265 is the scattering coefficient [30]. The surface areas, pore sizes, and pore volumes of the samples have been measured using the BET method by $N_2$ adsorption and desorption at 77 K in a micromeritics TriStar system. Transmission electron micrographs (TEM) were recorded digitally with a Gatan slow-scan

Table 1
Physicochemical and photocatalytic properties of the nanocrystalline $TiO_2$ materials obtained by the NSG method.

| Sample | $S_{BET}$[a] ($m^2\ g^{-1}$) | $V_p$[a] ($cm^3\ g^{-1}$) | $D_p$[a] (nm) | $d$[b] (nm) | $X_A$[c] (%) | Carbonaceous residues (mass%)[d] |
|---|---|---|---|---|---|---|
| NSG-AS | 284 | 0.38 | 4.5 | 5 | 100 | 12 |
| NSG-300-3 | 87 | 0.26 | 7.8 | 8 | 100 | 6.2 |
| NSG-400-1 | 70 | 0.22 | 9.5 | 11 | 100 | 4.1 |
| NSG-400-3 | 72 | 0.24 | 10 | 12 | 100 | 1.4 |
| NSG-400-8 | 69 | 0.23 | 9.8 | 12 | 100 | 0.51 |
| NSG-400-12 | 67 | 0.21 | 9.9 | 13 | 100 | 0.42 |
| NSG-500-1 | 64 | 0.20 | 12 | 18 | 100 | 2.8 |
| NSG-500-2 | 63 | 0.23 | 13 | 18 | 100 | 0.98 |
| NSG-500-8 | 62 | 0.23 | 13 | 19 | 100 | 0.22 |
| NSG-600-1 | 48 | 0.18 | 16 | 25 | 100 | 0.58 |
| NSG-600-3 | 47 | 0.18 | 17 | 26 | 100 | 0.04 |
| NSG-600-8 | 44 | 0.17 | 17 | 26 | 99 | 0 |
| NSG-700-3 | 12 | 0.06 | 20 | 30 | 54 | 0 |
| NSG-800-3 | 2 | 0.01 | 40 | 32 | 6 | 0 |
| P-25[e] | 55 | 0.21 | 19 | 25 | 70 | 0 |

[a] BET surface area ($S_{BET}$), average pore volume ($V_p$) and average pore diameter ($D_p$) of the NSG-derived $TiO_2$ samples estimated from nitrogen adsorption.
[b] Average size of anatase titania nanoparticles estimated from Scherrer equation.
[c] Ratio of anatase to rutile based on XRD data.
[d] The content of carbonaceous residues in the samples obtained from the TG data based on the weight loss between 200 and 700 °C [36].
[e] Commercial sample of Degussa P-25.

charge-coupled device (CCD) camera on a JEOL 2011 electron microscope operating at 200 kV. The samples for electron microscopy were prepared by grinding and subsequent dispersing the powder in acetone and applying a drop of very dilute suspension on carbon-coated grids. Simultaneous thermal gravimetric (TG/DTG) and differential thermal analysis (DTA) measurements were performed on a Perkin-Elmer 7series thermal analyzer apparatus in air flow (50 mL/min), using $Al_2O_3$ as a reference and with a heating rate of 10 °C/min. For each experiment, 10–15 mg of sample was used. X-ray photoelectron spectroscopy (XPS) spectra were recorded with a Perkin Elmer PHI 5000C system equipped with a hemispherical electron energy analyzer. The spectrometer was operated at 15 kV and 20 mA, and an aluminum anode (Al Kα, $h\nu$ = 1486.6 eV) was used. The C 1s line (284.6 eV) was used as the reference to calibrate the binding energies (BE).

### 2.3. Photocatalytic activity measurement

The laboratory irradiation experiments were performed in a self-constructed photoreactor consisting of a cylindrical quartz flask (diameter 40 mm, length 140 mm) placed in the middle of an internal aluminum-foil lined steel cylinder. The temperature of suspension system was controlled around 25 ± 0.5 °C by circulating cooling water. The used source of UV irradiation was four 8 W UV lamps (located at 5 cm around the quartz flask) with the characteristic emission wavelength of 310 nm.

Phenol ($C_6H_5OH$) is a common chemical that is used extensively in a variety of industrial applications. Therefore, it is chosen to be as a model pollutant. Briefly, an amount of 50 mg of the catalyst was dispersed in 150 ml of the phenol (SCR, 99%) aqueous solution ($C_0$ = 0.60 mmol $L^{-1}$, pH 7). Before use, $TiO_2$ suspension was sonicated for 5 min with a sonicator (Brandson, 240 W/2 KHz) and then magnetically stirred for about 30 min under the condition of oxygen bubbling (50 mL $min^{-1}$) in dark to achieve the adsorption/desorption equilibrium. At regular irradiation intervals, the dispersion was sampled and examined by HPLC (Shimadzu device with LC-10ATvp Pump and SPD-10Avp UV–vis detector) analysis to calculate the phenol degradation yield (%). Meanwhile, experimental results also confirmed that only less than 5% phenol decomposed after reaction for 2 h under the same conditions in the absence of either the photocatalyst or the UV light and thus, could be neglected in comparison with that in the presence of both the catalyst and the UV source. After reaction, the catalyst was collected by centrifugation and washed by distilled water under sonication. Then the catalyst was dried and collected to do the durability experiment.

## 3. Results

### 3.1. Measurements of XRD, TEM and $N_2$ adsorption

Fig. 1 presents the XRD patterns of the as-prepared and calcined NSG-$TiO_2$ samples. It is seen that the as-synthesized sample shows well-defined diffraction peaks characteristic of anatase titania. The significant amount of peak broadening as observed is due to the nanocrystalline nature of the as-synthesized $TiO_2$. Upon calcination at elevated temperatures from 300 to 600 °C, a progressive enhancement of the crystallization degree of the anatase phase is identified, as reflected from a continuous sharpening and intensification of the diffraction peaks for the calcined samples as shown in Fig. 1. Moreover, from a comparison of the diffraction peaks in the 600 °C-calcined samples for various times, one can find that NSG-600-8 obtained by calcination at 600 °C for extended time of 8 h exhibited several new weak diffraction peaks corresponding to rutile phase, suggesting the occurring of a slight

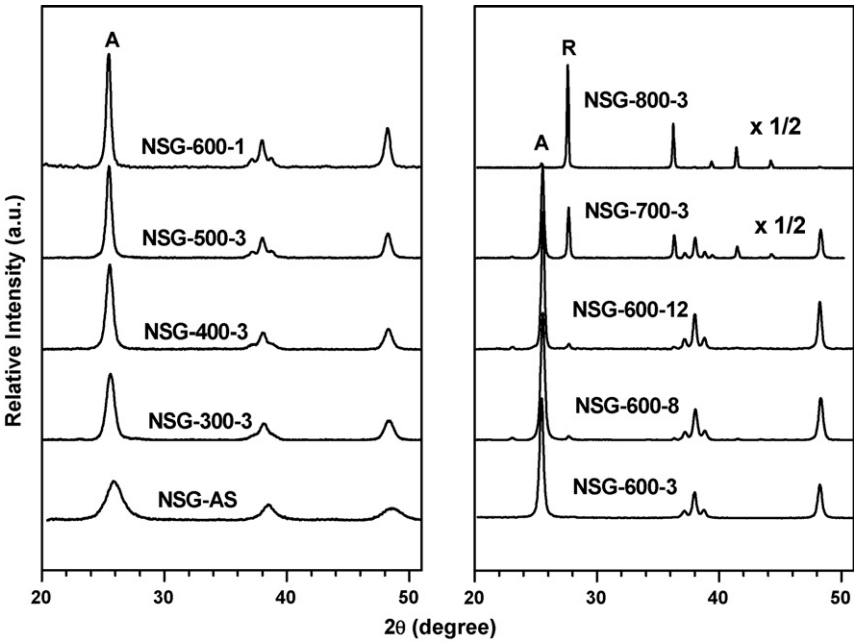


Fig. 1. XRD patterns of the NSG-derived nanocrystalline $TiO_2$ samples calcined at various temperatures. The peaks marked A and R represent the anatase and rutile phase, respectively.

transformation of the anatase to rutile phase by extending the calcination times at 600 °C. This unambiguously demonstrates that apart from the calcination temperature, the calcination time also plays an essential role in controlling the phase transformation behavior of the present NSG-derived $TiO_2$ samples. After calcination in air at 700 °C for 3 h, the sample displays a significant transformation of anatase into rutile phase. Further calcination of the samples at temperatures above 800 °C results in the total replacement of anatase by rutile phase for the $TiO_2$ materials. The marked difference in the ratio of anatase and rutile phases as well as the average crystallite sizes for as-synthesized or calcined $TiO_2$ samples has been tabulated in Table 1, showing that an effective control of the crystallite size as well as nanocrystalline phase can be achieved for the present NSG-derived samples.

Transmission electron microscopy (TEM) was used to further examine the crystallite/particle size, the crystallinity and morphology of the as-synthesized and calcined $TiO_2$ samples derived by the NSG method. It is found that the as-synthesized $TiO_2$ sample (Fig. 2a) is highly porous in nature and the average size of the primary particles is around 5 nm, which is in good agreement with the value determined by XRD. Image at higher magnification (Fig. 2a, inset) shows sets of lattice fringes, giving evidence the highly crystalline nature of the particles. The selected-area diffraction pattern (Fig. 2a, inset) for the NSG-AS sample indexes to anatase, in agreement with the X-ray diffraction data. It is noticeable that the presence of appreciable amount of amorphous domains makes it rather difficult to distinguish the boundaries of the particles clearly, showing evidence the inherently semicrystalline nature of the as-synthesized $TiO_2$ sample. After being thermally treated at 400 °C for 3 h, loosely aggregated nanoparticles with the same particle size around 11–14 nm were observed for the NSG-400-3 sample (Fig. 2b). This indicates that the nanosized particles have grown markedly during the calcination. After a further calcination at 600 °C, larger particles (20–25 nm) and even big lumps were observed for the NSG-600-3 sample (Fig. 2c).

The specific surface area ($S_{BET}$) and the cumulative pore volume of the as-synthesized $TiO_2$ sample (i.e. NSG-AS) have been measured to be 284 $m^2\ g^{-1}$ and 0.38 $cm^3\ g^{-1}$, respectively (shown in Table 1). The pore size distribution measurements show that a well-developed mesostructure was achieved for the NSG-AS sample, which exhibits a narrow pore size distribution in the range of 3–5 nm. The effect of the calcination temperature on specific surface area for the present as-synthesized sample is dramatic as reported for conventional aqueous sol–gel-derived $TiO_2$ materials in the literature [31]. It is seen that the $S_{BET}$ of the calcined $TiO_2$ is significantly lower than that of the as-synthesized sample and decreases continuously from 87 to 44 $m^2\ g^{-1}$ with increasing calcination temperature in the range of 300–600 °C. Owing to sintering and phase transformation of anatase to rutile, at 700 and 800 °C, the specific surface area decreases drastically to ca. 12 (NSG-700-3) and 2 $m^2\ g^{-1}$ (NSG-800-3), respectively. The variation of the sample pore volume, with the calcination temperature, followed the same trend of the surface area.

### 3.2. Measurements of diffuse reflectance FTIR spectroscopy (DRIFTS), TG-DTA and XPS

It is well known that metal oxides obtained by NSG methods could often contain a certain amount of organic compounds or carbonaceous residues [32]. DRIFTS has been employed to follow the variation of the surface properties of the as-synthesized sample NSG-AS as a function of calcination temperature (Fig. 3). The spectra for all samples show one

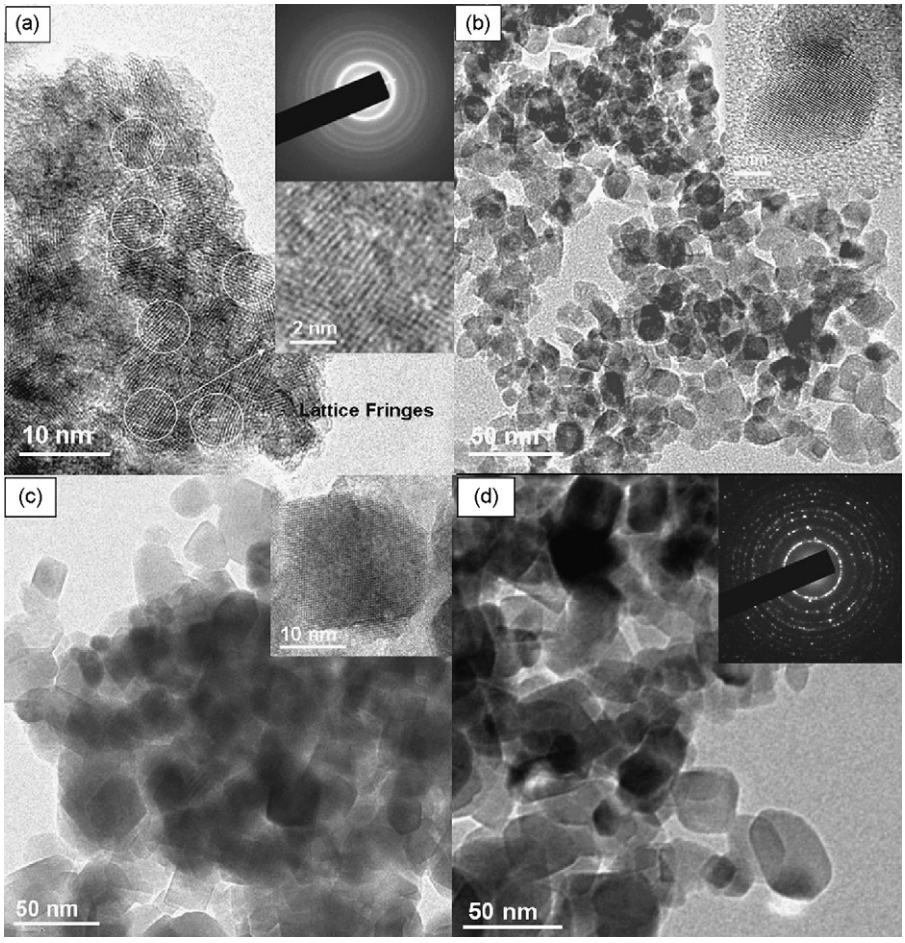


Fig. 2. TEM images of the $TiO_2$ samples. (a) NSG-AS, (b) NSG-400-3, (c) NSG-600-3, (d) Degussa P-25. Inset shows the SAED patterns and HRTEM images.

broad band near 3300 $cm^{-1}$ and another one near 1625 $cm^{-1}$ which corresponds to surface-adsorbed water and hydroxyl groups [33]. The IR absorption in the spectral range of 600–1000 $cm^{-1}$ has been assigned to the surface vibrations of the Ti–O bonds [34]. As shown in Fig. 3, the as-synthesized $TiO_2$ sample has more surface-adsorbed water and hydroxyl groups than annealed samples. Moreover, the IR spectra of the as-synthesized sample (Fig. 3a) shows significant peaks at ca. 3011, 2909, 1504, and 1441 $cm^{-1}$ corresponding to the remaining aromatic organic-moiety remaining on the surface of the as prepared samples, which practically disappears after thermal treatment. Notice that the spectra for samples NSG-300-3 and NSG-400-3 show much weaker vibrational features around 3000 $cm^{-1}$, suggesting the presence of only trace amount of organic residues in these samples. Further calcination at 500 °C results in the total disappearance of the absorption features around 3000 and 1500 $cm^{-1}$ in spectra of Fig. 3d, demonstrating the ''clean'' surface nature for the NSG sample calcined at 500 °C for 3 h. In addition, absorption peak associated with the stretching vibration mode of isolated OH groups (nearly 3643 $cm^{-1}$) were also observed for calcined samples [33].

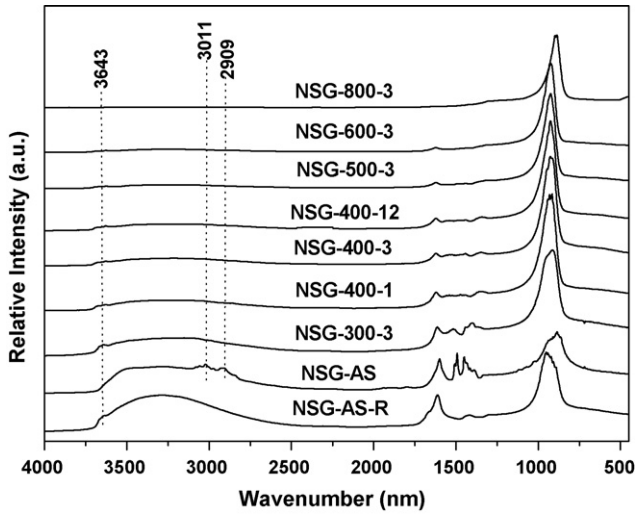


Fig. 3. DRIFT Spectra of the as-synthesized (NSG-AS) and calcined $TiO_2$ materials. For comparison purposes, the spectrum of the NSG-AS sample after one photocatalytic run (NSG-AS-R) is also included.

Fig. 4 shows the simultaneous TG/DTA profiles under flowing air for sample NSG-AS. The first endotherm peak at ca. 48 °C is attributed to the loss of residual organics or physisorbed water from. This peak occurs concurrently with a moderate TG weight loss of 4%. The second DTA peak, a broad exotherm tailed to 350 °C with a maximum at ca. 238 °C, may be due to oxidation of residual organic compounds chemically bonded to the surface of the as-synthesized $TiO_2$ sample and corresponds to a gradual weight loss of 11%. Two

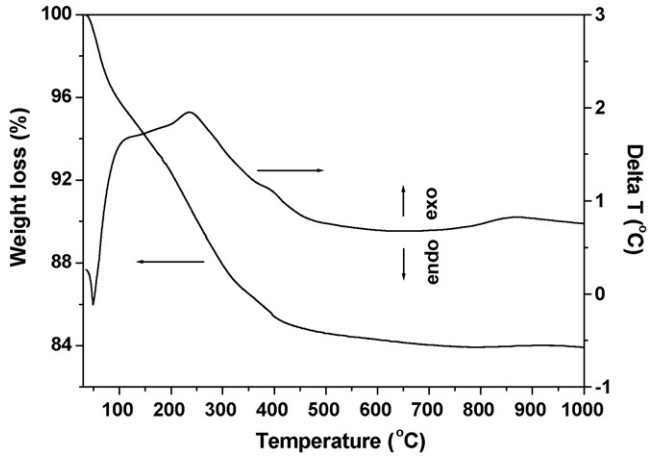


Fig. 4. Thermal analysis (TG/DTA) profiles of the as-synthesized NSG-$TiO_2$ sample (10 °C $min^{-1}$ ramp under 20 mL $min^{-1}$ flowing air).

additional exotherms occur with maxima at 400 and 870 °C and a combined weight loss of 1%. The total mass loss for the NSG-AS sample heated to 1000 °C, as determined by TG analysis, was 16%, the majority of which occurred between 120 and 400 °C (ca. 11%, see Table 1).

Thermogravimetric measurements (TG/DTA) were also performed to gain information on the surface residues of those samples calcined at temperatures ranging from 300 to 800 °C. Based on the weight loss between 200 and 700 °C, the amount of carbonaceous residues remained on the surface of the calcined samples is found to be strongly dependent on the calcination temperature and calcination time as shown Table 1. It is clear that the samples calcined at relatively lower temperatures of 300 and 400 °C contain considerable amount of carbon residue. The presence of such an appreciable amount of carbon suggests an incomplete decomposition of the surface organic residue at these temperatures, which will be further discussed by XPS analysis.

The XPS has been used to investigate oxygen deficiencies in the NSG-$TiO_2$ samples. Fig. 5 shows O 1s, Ti 2p and C 1s core level XPS spectra of the NSG-$TiO_2$ samples calcined at various temperatures. In literature, the O 1s peak is often believed to be composed of 3–5 different oxygen species, such as Ti–O bonds in $TiO_2$ and $Ti_2O_3$, hydroxyl groups, C–O bonds, and adsorbed $H_2O$ [35]. To get reliable data and statistics, the O 1s peak is modeled with two pseudo-Voigt functions [36]. In Fig. 5 (O 1s), the O 1s signal shows two contributions at 530.1 and 532.3 eV after peak modeling. The main peak at ca. 530.1 eV could be ascribed to lattice oxygen in $TiO_2$, while the signal at ca. 532.3 eV could be associated to surface hydroxyl groups [37,38]. The evolution of the Ti 2p signal during calcination was also clearly shown in Fig. 5 (Ti 2p) indicating a decreasing "shadowing effect" of the surface organic residue for NSG-300-3 and NSG-400-3 samples, leading to a less intense Ti 2p signal in the precursor calcined at lower temperatures. This effect confirms the progressive removal of the organic moieties covering the surface for the original as-synthesized sample. Moreover, one additional peak located at ca. 456.2 eV ascribed to $Ti^{3+}$ $2p_{3/2}$ could be identified in as-prepared sample and the samples calcined under mild condition [39]. For the sample

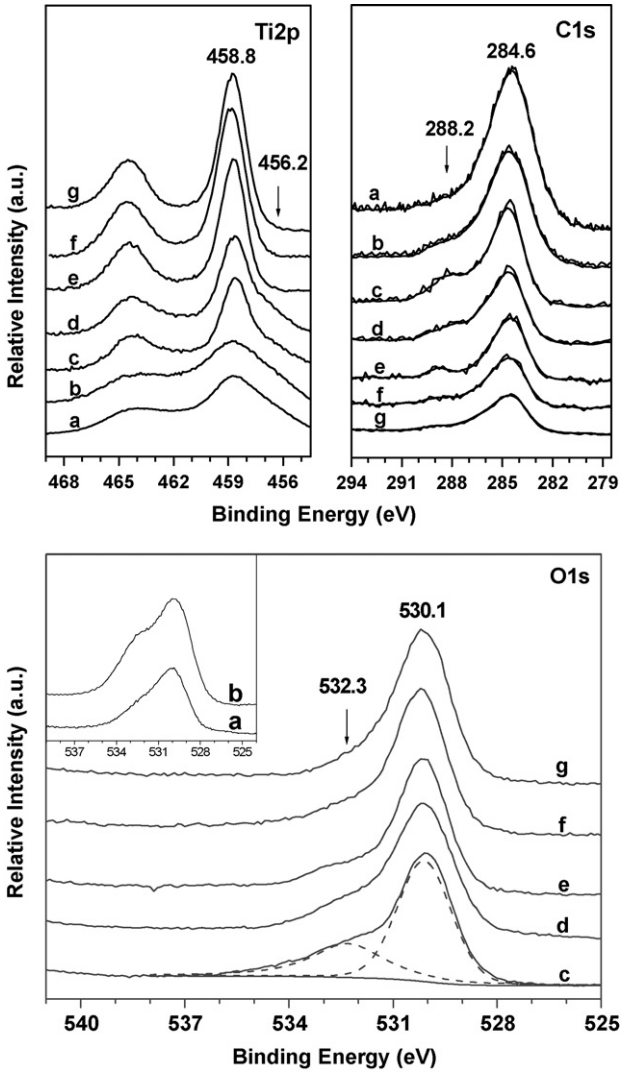


Fig. 5. XPS spectra of various NSG-$TiO_2$ samples obtained by the NSG method. (a) NSG-AS, (b) NSG-300-3, (c) NSG-400-1, (d) NSG-400-3, (e) NSG-400-8, (f) NSG-500-3, (g) NSG-600-3.

NSG-400-8, nearly no shoulder peak at ca. 456.2 eV was found, suggesting the total removal $Ti^{3+}$ species in further calcined samples. More complex situation was observed for C 1s photoemissions in Fig. 5, where two types of carbon species were detected. The main species in the NSG-$TiO_2$ samples, with bind energy at 284.6 eV, are associated with the organic residues either from the benzyl alcohol precursor or from the graphitic carbon species due to surface contamination. An additional weak but well-defined feature at 288.2 eV could be attributed to more oxidized species, for example carboxilates [40]. A close comparison of the evolution of this feature for different NSG samples reveals an initial increase followed by subsequent disappearance of the photoemission at 288.2 eV. This indicates that elimination of carbon residue occurs through a partial oxidative pyrolysis pathway.

Based on the area integral of the two peaks corresponding to lattice oxygen ($O_L$) and surface hydroxyl ($O_{OH}$) of O 1s photoemissions, the ratio of $O_{OH}$ to $O_T$ ($O_T = O_{OH} + O_L$) for all samples was calculated as shown in Table 2 [36]. It can be

Table 2
Summary of the XPS data for various NSG-$TiO_2$ samples

| Samples | $O_T$/Ti | $O_L$/Ti | $O_{OH}/O_T$[a] (%) |
|---|---|---|---|
| NSG-AS | 2.45 | 1.59 | 35 |
| NSG-300-3 | 2.59 | 1.30 | 51 |
| NSG-400-1 | 2.43 | 1.70 | 30 |
| NSG-400-3 | 2.34 | 1.71 | 27 |
| NSG-400-8 | 2.25 | 1.78 | 21 |
| NSG-500-3 | 2.11 | 1.81 | 14 |
| NSG-600-3 | 2.07 | 1.84 | 11 |
| NSG-700-3 | 1.97 | 1.92 | 4.2 |
| NSG-800-3 | 1.98 | 1.96 | 2.1 |

[a] Ratio of $O_{OH}$ and $O_T$ was calculated from area integral of $O_{OH}$ and $O_L$ in O1s XPS spectra ($O_T = O_{OH} + O_L$) [38].

noticed that the intensity ratio of $O_{OH}/O_T$ continuously decreases with increasing calcination temperature/time, indicating the progressive loss of the surface hydroxyl species. After calcination at 700 °C for 3 h, a drastic decrease of the ratio of $O_{OH}/O_T$ to 4.2% was observed. The surface composition calculated from the XPS data is also summarized in Table 2. Because of the additional presence of graphitic contaminations in the XPS measurement, the amount of surface carbon atoms was not calculated. Noteworthy is that an increase in the ratio of $O_L$/Ti to a stoichiometric value of 2 with increasing calcination temperatures is observed, thus further confirming the presence of oxygen deficiencies over the low-temperature calcined NSG-$TiO_2$ samples.

### 3.3. Measurement of photocatalytic activity

The photocatalytic degradation of phenol has been chosen as a model reaction to evaluate the photocatalytic activities of the present NSG-$TiO_2$ catalysts. Fig. 6 shows the evolution curves of photocatalytic degradation of phenol on commercial Degussa P-25 powders as well as the various $TiO_2$ samples obtained by calcination at different temperatures for 3 h. All samples showed catalytic activity in phenol degradation reactions strongly depending on the calcination temperature. It is important to note that the low-temperature as-synthesized sample NSG-AS exhibits considerable activity in terms of photodegradation yield of phenol, revealing a photocatalytic activity quite comparable with that of the commercial photocatalyst Degussa P-25 as shown in Fig. 6. Additionally, it is seen that the photocatalytic activity of the NSG-$TiO_2$ samples can be further markedly enhanced by subsequent calcination at elevated temperatures ranging from 300 to 600 °C. Notice that the NSG-400-3 sample obtained by calcination at 400 °C for 3 h exhibits the highest activity, which also appears to be far superior to the commercial Degussa P-25 for photocatalytic degradation of phenol. Moreover, with increasing calcination temperature from 400 to 800 °C, a rapid decrease in the activities was observed. Among all the NSG-$TiO_2$ catalysts tested, sample NSG-800-3, which has very low surface area and is composed of large crystallites in the rutile phase, affords the lowest photoactivity for phenol degradation.

To gain a further insight into the effect of calcination time on the photocatalytic activity of the NSG-derived anatase $TiO_2$, the plot of the phenol removal rates obtained over a series of 400–600 °C calcined NSG-$TiO_2$ samples, versus corresponding calcination time ranging from 1 to 8 h is shown in Fig. 7. Again, it is seen that in most cases, the photocatalytic activities of the 400 °C-calcined samples are much higher than the samples calcined at either lower or higher temperatures. Noticeably, a significantly different variation behavior of the photoactivity as a function of calcination time has been observed in the samples calcined at three different temperatures, demonstrating that apart from calcination temperature, the calcination time also plays a key role in determining the photoactivity of the present NSG-$TiO_2$ samples. A close comparison of the variation behavior of the photoactivity of the NSG-$TiO_2$ samples calcined at temperatures of 300–600 °C further reveals that the higher the calcination temperature, the less calcination time

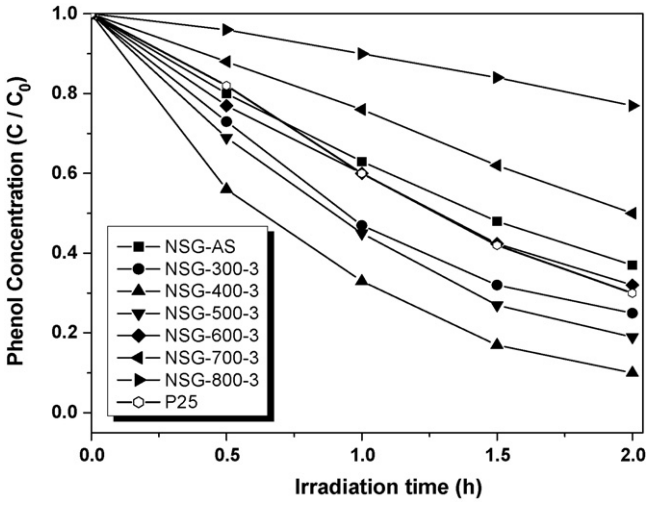


Fig. 6. Photocatalytic degradation of phenol on various NSG-derived $TiO_2$ samples calcined at different temperature. For comparison purposes, the evolution curve of the commercial photocatalyst of Degussa P-25 powder is also included.

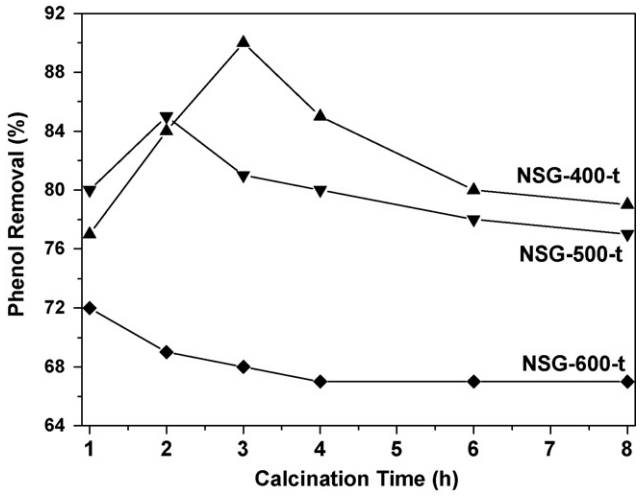


Fig. 7. Photocatalytic degradation rate of phenol on 400, 500, and 600 °C calcined NSG-$TiO_2$ samples as a function of calcination time.

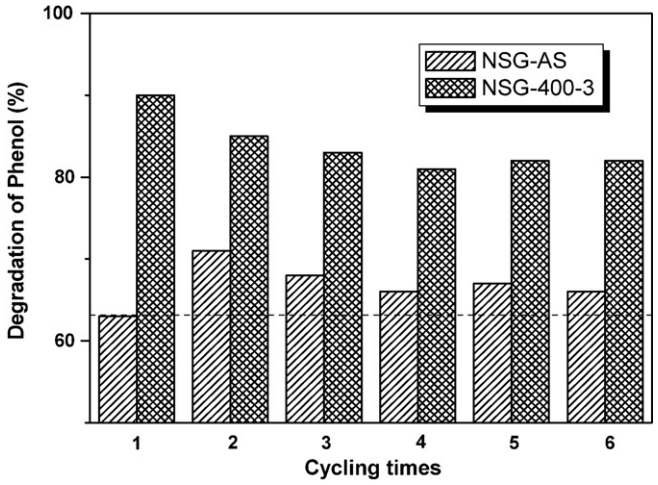


Fig. 8. Reusability of sample NSG-AS and NSG-400-3.

is needed for achieving the highest photoactivity for the NSG-$TiO_2$ samples. In the case of the 400 °C-calcined samples, the highest catalytic activity was observed for the NSG-400-3 sample prepared by calcination at 400 °C for 3 h.

The photocatalytic activity in phenol degradation obtained on sample NSG-AS and NSG-400-3 after different reuses is presented in Fig. 8. Noteworthy is that, after the first reuse, a markedly enhanced photocatalytic activity is observed for the recycled NSG-AS samples. Moreover, the enhanced photocatalytic activity of the NSG-AS samples could be maintained even after six recyclings and reuse of the catalyst. In contrast, the NSG-400-3 samples exhibiting a much higher photocatalytic activity during the first cycle, experience a continuous deactivation during the recycling tests. The observed results clearly evidenced the remarkably different durability of the two samples for prolonged photo irradiation.

## 4. Discussion

Previous investigations concerning the surface preparation of $TiO_2$-based materials for photocatalytic applications have revealed that the generation of a clean surface, free of contamination by organic species is highly important for attaining a high activity of a $TiO_2$ photocatalyst [41]. It is interesting to note that the present as-synthesized nanocrystalline sample NSG-$TiO_2$-AS is evidenced to be surface-capped with appreciable amount of organic moieties, which however exhibits considerable activity comparable to that of commercial photocatalyst Degussa P-25 during the photocatalytic degradation of phenol. According to a recent investigation by Kanaev et al., a surface activation by a UV-assisted exchange between the surface organic moieties and surface hydroxy groups during the photocatalytic process may play a key role in achieving the high performance of a series of propoxy-capped $TiO_2$ catalysts [42]. In our case, the evolution of the surface features of the NSG-AS sample with respect to sample NSG-AS-R during the reaction as demonstrated by the DRIFT results unambiguously indicates that disappearance of the organic traces could take place at the initial stage of the reaction (Fig. 3), thus leading to the *in situ* generation of ''clean'' surface in the active catalyst. Meanwhile, the clear enhancement of stretching mode of Ti–OH bonds (nearly 3643 $cm^{-1}$) was also observed for NSG-AS-R with respect to sample NSG-AS, which means more surface hydroxyl groups are formed due to the efficient *in situ* removal of surface-capped organic species. It is well established that surface hydroxyl groups play an important role in the photocatalytic process because the photoinduced holes can attack those surface hydroxyl groups and yield surface hydroxyl radicals with high oxidation capability [43]. Therefore, it is reasonable that a considerable performance for photodegradation of phenol could be achieved with the present organic-capped nanocrystalline NSG-AS sample.

In terms of the photocatalytic efficiency, subsequent thermal treatment of the as-synthesized sample NSG-AS at elevated temperatures ranging from 300 to 600 °C was beneficial and a further enhancement in phenol degradation as a consequence of a progressive elimination of the surface organic residue along with a further crystallization in the anatase phase. However, the best photocatalytic activity has been reached with the sample calcined at 400 °C for 3 h. Spectroscopic characterization of the present NSG-$TiO_2$ materials as a function of subsequent calcination, using DRIFTS, XRD, XPS, reveals that calcination at temperatures above 300 °C provokes the elimination of surface organic residue. This elimination may induce the formation of surface oxygen deficiency in the structure, acting as electron trapping center, which could improve the photocatalytic activity [40,44]. Thus, the samples calcined at temperatures lower than 600 °C consist in a well-crystallized anatase, with high specific surface area and with certain intermediate states produced by the existence of oxygen deficiencies which appear to be responsible for the high efficiency of the calcined photocatalysts.

Regarding the effect of particle size on the photocatalytic performance of anatase $TiO_2$, it is well documented that a reduction in the particle size of anatase $TiO_2$ can usually lead to an enhancement in its activity for the photocatalytic degradation of organic pollutants [4]. It is believed that enhanced quantum yields is achievable for the nanosized catalysts due to more efficient transfer of the photo-generated charge carriers from the interior to the particle surface [42,45]. It appears that this is true for the present calcined NSG-$TiO_2$ samples with calcination temperatures lower than 600 °C. However, this rationalization does not explain the impact of calcination time on the performance of the 400, 500 and 600 °C-calcined samples. As seen in Fig. 7 and Table 1, the much higher photoactivity of sample NSG-400-3 as compared to its other 400 °C-calcined counterparts is not consistent with their similar particle sizes in the anatase phase. Taking into account the quite similar particle sizes for the NSG-400-*t* samples, we consider that, besides the evolution and variation of the microstructural properties as discussed above, the amount of carbonaceous residues on the samples could be a significant factor affecting the photocatalytic activity.

Concerning this, it is important to point out that the low temperature calcined NSG-$TiO_2$ samples are evidenced to be

surface-capped with appreciable amount of carbonaceous residues. The fact that the photocatalytic activities of sample NSG-300-3 are lower than that of NSG-400-3 is in accordance with previous predictions that the significant amount of carbonaceous residues occluded in the $TiO_2$-based photocatalysts derived by NSG route is always detrimental to the overall photoactivities [41]. While prolonged calcination at temperatures higher than 400 °C is needed to completely eliminate the carbonaceous residues existed in the catalysts, it is noteworthy that presence of appropriate amount of carbonaceous residues is beneficial for the enhanced performance of the NSG-400-*t* and NSG-500-*t* samples as reported in Fig. 7. A recent investigation of the surface modification of a $TiO_2$ photocatalyst by Tryba et al. has shown that commercially available $TiO_2$ (ST-01) can be photosensitized by mixing $TiO_2$ with polyvinyl alcohol followed by pyrolysis at suitable temperatures and such photosensitization effect can improve the photocatalytic activity [41].

At this situation, it is interesting to note that the most active NSG-400-3 catalyst has a different type of carbonaceous species with respect to that of sample NSG-AS, inferring that the specific form of carbonaceous species also plays an important role in determining the photocatalytic activity. Spectroscopic characterization by DRIFTS and XPS reveals that the residual species on sample NSG-AS are mainly easily removed surface-capped organic moieties. However, more oxidized species, for example carboxilates firmly attached to sample surface, were identified on the calcined NSG-400-3 sample. As a result, the markedly different durability was identified for the NSG-AS and NSG-400-3 samples subjected to prolonged photoirradiation (Fig. 8). Therefore, the present observations unambiguously demonstrate that apart from the microstructural properties, the carbonaceous residues of the catalyst also play an important role in the photocatalytic performance of present NSG-derived $TiO_2$-based materials.

## 5. Conclusions

In the present work, we have successfully demonstrated that highly photoactive nanocrystalline anatase $TiO_2$ photocatalysts with tailored surface and microstructural properties can be obtained by a facile NSG method based on solution-based reaction between $TiCl_4$ and benzyl alcohol at near ambient temperature. It has been shown for the first time that the organic-capped nanocrystalline $TiO_2$ sample as-obtained at low temperature exhibits considerable activity toward photodegradation of phenol. Moreover, it is demonstrated that the photocatalytic activities of the as-prepared nanocrystalline $TiO_2$ sample can be further markedly enhanced by subsequent thermal treatment at elevated temperatures. Combined spectroscopic characterizations by DRIFTS, DR UV–vis and XPS show that both the calcination temperature and calcination time are important parameters in controlling the surface nature and the microstructural properties of the calcined $TiO_2$ samples, with the highest photoactive $TiO_2$ sample obtained by calcination at 400 °C for 3 h appears to be far superior to that of the commercial photocatalyst Degussa P-25.

## Acknowledgements

The financial supports from National natural science foundation of China (Grant No. 20473021, 20421303, 20633030), the national key basic research program (Grant No. 2003CB615807), the research fund for the doctoral program of higher education (Grant No. 20050246071), and the national high technology research and development program of China (2006AA03Z336) are gratefully acknowledged.

## Reference

[1] A. Fujishima, T.N. Rao, D.A. Tryk, J. Photochem. Photobiol. C 1 (2000) 1.
[2] A.L. Linsebigler, G. Lu, J.T. Yates Jr., Chem. Rev. 95 (1995) 735.
[3] X.Y. Deng, Y.H. Yue, Z. Gao, Appl. Catal., B 39 (2002) 135.
[4] A.J. Maira, K.L. Yeung, J. Soria, J.M. Coronado, C. Belver, C.Y. Lee, Appl. Catal., B 29 (2001) 327.
[5] D.M. Antonelli, Microporous Mesoporous Mater. 30 (1999) 315.
[6] P.C.A. Alberius, K.L. Frindell, R.C. Hayward, E.J. Kramer, G.D. Stucky, B.F. Chmelka, Chem. Mater. 14 (2002) 3284.
[7] J.C. Yu, X.C. Wang, X.Z. Fu, Chem. Mater. 16 (2004) 1523.
[8] P.W. Morrison, J.R. Raghavan, A.J. Timpone, C.P. Artelt, S.E. Pratsinis, Chem. Mater. 9 (1997) 2702.
[9] Y. Murakami, T. Matsumoto, Y. Takasu, J. Phys. Chem. B 103 (1999) 1836.
[10] A. Zaban, S.T. Aruna, S. Tirosh, B.A. Gregy, Y. Mastai, J. Phys. Chem. B 104 (2000) 4130.
[11] K.N.P. Kumer, K. Keizer, A.J. Burggraaf, T. Okubo, H. Nagamoto, S. Morooka, Nature 358 (1992) 48.
[12] S. Ito, S. Inoue, H. Kawada, M. Hara, M. Iwasaki, H. Tada, J. Colloid Interface Sci. 216 (1999) 59.
[13] C.H. Lu, S.K. Saha, J. Sol–gel Sci. Technol. 20 (2001) 27.
[14] S. Kobayashi, K. Hanabusa, M. Suzuki, M. Kimura, H. Shirai, Chem. Lett. 10 (1999) 1077.
[15] A.E. Gash, T.M. Tillotson, J.H. Satcher, J.F. Poco, L.W. Hrubesh, R.L. Simpson, Chem. Mater. 13 (2001) 999.
[16] T.Y. Yu, J. Joo, Y.I. Park, T. Hyeon, Angew. Chem. Int. Edit. 44 (2005) 7411.
[17] G.W. Koebrugge, L. Winnubst, A.J. Burggraaf, J. Mater. Chem. 3 (1993) 1095.
[18] J.C. Yu, J.G. Yu, W.K. Ho, L.Z. Zhang, Chem. Commun. (2001) 1942.
[19] C.C. Wang, J.Y. Ying, Chem. Mater. 11 (1999) 3113.
[20] R.S. Davidson, C.L. Morrison, J. Abraham, J. Photochem. 24 (1984) 27.
[21] Z.S. Guan, X.T. Zhang, Y. Ma, Y.A. Cao, J.N. Yao, J. Mater. Res. 16 (2001) 907.
[22] J.C. Yu, L.Z. Zhang, J.G. Yu, Chem. Mater. 14 (2002) 4647.
[23] M.R. Hoffmann, S.T. Martin, W. Choi, D.W. Bahnemann, Chem. Rev. 95 (1995) 69.
[24] A. Matsuda, T. Matoda, T. Kogure, K. Tadanaga, T. Minami, M. Tatsumisago, J. Sol–gel Sci. Technol. 27 (2003) 61.
[25] P. Arnal, R.J.P. Corriu, D. Lecelercq, P.H. Mutin, A. Vioux, Chem. Mater. 9 (1997) 694.
[26] V. Lafond, P.H. Mutin, A. Vioux, J. Mol. Catal. A: Chem. 81 (2002) 182.
[27] P. Arnal, R.J.P. Corriu, D. Lecelercq, P.H. Mutin, A. Vioux, J. Mater. Chem. 6 (1996) 1925.
[28] G.Q. Guo, J.K. Whitesell, M.A. Fox, J. Phys. Chem. B 109 (2005) 18781.
[29] M. Niederberger, M.H. Bartl, G.D. Stucky, Chem. Mater. 14 (2002) 4364.
[30] H. Zhang, J.F. Banfield, J. Phys. Chem. B 104 (2000) 3481.
[31] H.X. Li, J. Zhu, G.S. Li, Y. Wan, Chem. Lett. 33 (2004) 574.
[32] J. Joo, S.G. Kwon, T. Yu, M. Cho, J. Lee, J. Yoon, T. Hyeon, J. Phys. Chem. B 109 (2005) 15297.
[33] Y. Kuroda, T. Mori, K. Yagi, N. Makihata, Y. Kawahara, M. Nagao, S. Kittaka, Langmuir 21 (2005) 8026.
[34] J.G. Yu, H.G. Yu, B. Cheng, X.J. Zhao, J.C. Yu, W.K. Ho, J. Phys. Chem. B 107 (2003) 13871.
[35] J.G. Yu, X.J. Zhao, Q.N. Zhao, Thin Solid Films 379 (2000) 7.
[36] H. Jensen, A. Soloviev, Z.S. Li, E.G. Sogaard, Appl. Surf. Sci. 246 (2005) 239.

[37] W. Gopel, J.A. Anderson, D. Frankel, M. Jaehnig, K. Phillips, J.A. Schafer, G. Rocker, Surf. Sci. 139 (1984) 333.
[38] R.L. Kurtz, R. Stockbauer, T.E. Madey, E. Roman, J.L. Desegovia, Surf. Sci. 218 (1989) 178.
[39] H.M. Liu, W.S. Yang, Y. Ma, Y. Cao, J.N. Yao, J. Zhang, T.D. Hu, Langmuir 19 (2003) 3001.
[40] G. Colon, M.C. Hidalgo, G. Munuera, I. Ferino, M.G. Cutrufello, J.A. Navio, Appl. Catal., B 63 (2005) 45.
[41] B. Tryba, T. Tsumura, M. Janus, A.W. Morawski, M. Inagaki, Appl. Catal., B 50 (2004) 177.
[42] M. Benmami, K. Chhor, A.V. Kanaev, J. Phys. Chem. B 109 (2005) 19766.
[43] R.T. Myers, Inorg. Chem. 17 (1978) 952.
[44] I. Nakamura, N. Negishi, S. Kutsuna, T. Ihara, S. Sugihara, E. Takeuchi, J. Mol. Catal. A: Chem. 161 (2000) 205.
[45] Z.B. Zhang, C.C. Wang, R. Zakaria, J.Y. Ying, J. Phys. Chem. B 102 (1998) 10871.